RESEARCH ARTICLE

# Upward nitrate flux and downward particulate organic carbon flux under contrasting situations of stratification and turbulent mixing in an Arctic shelf sea

Ingrid Wiedmann[*], Jean-Éric Tremblay[†], Arild Sundfjord[‡] and Marit Reigstad[*]

Increased sea ice melt alters vertical surface-mixing processes in Arctic seas. More melt water strengthens the stratification, but an absent ice cover also exposes the uppermost part of the water column to wind-induced mixing processes. We conducted a field study in the Barents Sea, an Arctic shelf sea, to examine the effects of stratification and vertical mixing processes on 1) the upward nitrate flux (into surface layers <65 m) and 2) the downward flux of particulate organic carbon (POC) to ≤200 m. In the Arctic-influenced, drift ice-covered northern Barents Sea, we found a low upward nitrate flux into the surface layers (<0.1 mmol nitrate $m^{-2}$ $d^{-1}$) and a moderate downward POC flux (40–200 m: 150–250 mg POC $m^{-2}$ $d^{-1}$) during the late phase of a peak bloom. A 1-D residence time calculation indicated that the nitrate concentration in the surface layers constantly declined. In the Atlantic-influenced, ice-free, and weakly stratified southern Barents Sea a high upward nitrate flux was found (into the surface layers ≤25 m: >5 mmol nitrate $m^{-2}$ $d^{-1}$) during a post bloom situation which was associated with a high downward POC flux (40–120 m: 260–600 mg POC $m^{-2}$ $d^{-1}$). We suggest that strong wind events during our field study induced vertical mixing processes and triggered upwards nitrate flux, while a combination of down-mixed phytoplankton and fast-sinking mesozooplankton fecal pellets enhanced the downward POC flux. The results of this study underscore the need to further investigate the role of strong, episodic wind events on the upward nitrate and downward POC fluxes in weakly stratified regions of the Arctic that may be ice-free in future.

**Keywords:** nitrate flux; POC export; sediment trap; sedimentation; warming Arctic; space-for-time substitution

## 1. Introduction

The declining sea ice cover in Arctic seas (Arrigo and van Dijken, 2015; IPCC, 2013) affects the pelagic marine ecosystem in contrasting ways. Sea ice melt strengthens the water column stratification and hampers the upward nitrate flux into the surface layer (Tremblay et al., 2015), while an absent sea ice cover allows various wind-driven processes (e.g. wind-driven shear, breaking waves) to induce vertical mixing and shelf-break upwelling (Carmack and McLaughlin, 2011; Rainville et al., 2011; Falk-Petersen et al., 2015). Such mixing and upwelling can generate strong upward nitrate fluxes into the surface layers (Hales et al., 2005; Randelhoff et al., 2016). Dependent on the intensity of the nutrient renewal in the surface layer, the plankton abundance and composition may change, which in turn can modify the downward flux

of particulate organic carbon (POC). However, definitive regulating mechanisms of the POC flux are still under discussion (Carmack and Wassmann, 2006; Wassmann and Reigstad, 2011; Forest et al., 2013).

We conducted a field study in the Barents Sea, an Arctic shelf sea, to investigate the upward flux of nitrate and the downward flux of POC in contrasting field situations of ice cover, hydrography, mixing, and plankton abundance and composition. Arctic-derived water masses (temperature $T < 0°C$, salinity $S = 34.4–34.8$; Loeng, 1991) influence the northern Barents Sea, which is seasonally ice-covered (annual maximum extension found during March–April; Kvingedal, 2005). In late spring and summer, the sea ice recedes northwards and a phytoplankton bloom commonly occurs in the marginal ice zone, where the waters are well-lit and contain high, winter-accumulated, nutrient concentrations after the ice break-up. This bloom is often associated with a major downward POC flux, because senescent stages, resting stages and aggregates of diatoms, the often prevailing microalgae, have high sinking velocities (Eppley et al., 1967; Bienfang, 1981; Iversen and Ploug, 2013). In addition, an ice edge

[*] UiT The Arctic University of Norway, Tromsø, NO

[†] Québec-Océan and Takuvik, Biology Department, Université Laval, Québec City, Québec, CA

[‡] Norwegian Polar Institute, Tromsø, NO

Corresponding author: Ingrid Wiedmann (Ingrid.wiedmann@uit.no)

Art. 43, page 2 of 15

Wiedmann et al: Upward nitrate flux and downward particulate organic carbon flux under contrasting situations of stratification and turbulent mixing in an Arctic shelf sea

mesozooplankton community has been described to have lower ingestion rates than one in open waters (Wexels Riser et al., 2008). The result is a relatively low POC attenuation in the water column which may contribute to a greater downward POC flux at the ice edge (Wassmann and Reigstad, 2011).

The southern Barents Sea is influenced by Atlantic-derived waters ($T > 3°C$, $S > 35.0$; Loeng, 1991) and is ice-free the whole year. Accordingly, this region is prone to wind mixing, and the water column does not stratify before the sea surface warms in summer (Andreassen and Wassmann, 1998; Reigstad et al., 2002). Due to the absence of sea ice, the enhanced irradiance in surface waters allows the spring phytoplankton bloom to develop earlier than in the seasonally ice-covered northern Barents Sea (Leu et al., 2011). The phytoplankton bloom may thus peak at the ice edge during late June, while the southern Barents Sea already experiences a post-bloom period. The latter is commonly associated with an abundant meso-zooplankton community and enhanced ingestion rates (Wexels Riser et al., 2008), exhibiting a strong POC attenuation in the water column and causing a reduction of the POC export (Wassmann and Reigstad, 2011). However, previous studies also reported major downward POC fluxes in the deep mixed southern Barents Sea during late spring and early summer (Olli et al., 2002; Reigstad et al., 2008). Definitive drivers for this major flux have not been identified yet, but model results suggested that the downward POC flux may be linked to an enhanced upward nutrient flux caused by deep mixing events (Sakshaug and Slagstad, 1992; Sundfjord et al., 2007).

Here, we conducted a field study in the northern, drift ice-covered Barents Sea, the Polar Front, and the ice-free, southern Barents Sea. We assess in particular the link between mixing, upward nitrate flux and downward POC flux at the northernmost and southernmost study sites, because they contrasted in terms of stratification, turbulent mixing, phytoplankton bloom stage and zooplankton abundance. In this way, we could (1) compare the intensity of the upward nitrate flux, (2) study the contribution of this flux to the nitrate stock in the upper water column, and (3) investigate possible mechanisms for the regulation of the downward POC flux under contrasting regimes of hydrography, wind mixing, and spring phytoplankton bloom stage.

## 2. Materials and methods

Fieldwork was carried out in the Barents Sea with the ice-enforced R/V *Helmer Hanssen* (22–27 June 2011) as part of the Norwegian CONFLUX project. Based on a high resolution northward CTD-F transect along the 30°E longitude (S. Basedow, personal communication), four stations (M1–M4) were chosen for more detailed process studies. The hydrography, vertical mixing, suspended biomass and vertical export were assessed from the marginal ice zone in Arctic-influenced waters (M1), through the Polar Front (M2 and M3), and into Atlantic-influenced waters (M4; **Figure 1**, **Table 1**). These parameters gave important insight into the gradual change in the physical and biological environment from north to south motivating

us to assess the link between the upward nitrate flux and the downward POC flux at the two most contrasting sites (M1 and M4; **Figure 1**).

### 2.1 Hydrography, sea ice, light conditions, and wind

Physical variables (temperature, salinity) and fluorescence data were obtained at each station from surface to bottom (CTD-F, SeaBird 911*plus*) and processed with the SeaBird standard software package (bin average 0.5 m). Following Brainerd and Gregg (1995), we use the term 'mixed layer' for the weakly stratified surface layer, which was not necessarily actively mixed during the time of data collection. In contrast, we use 'mixing layer' to denote the surface depth interval that was actively mixed with a diffusivity $>10^{-4}$ $m^2$ $s^{-1}$ during data collection (Wiedmann et al., 2014). Due to our focus on the vertical transport of nitrate and organic matter, we use the term 'mixing layer' instead of the recently suggested term 'turbulent layer' (Franks, 2015). The sea ice conditions were estimated visually based on the scale of the Norwegian Meteorological Institute (11 categories from ice-free to fast ice). The underwater irradiance was measured with a multispectral GMBDH TRIOS light sensor (190–575 nm, 2.15 nm wavelength resolution) at each station between the air-sea interface and 20 m during local noon. The base of the euphotic zone (1% subsurface irradiance) was calculated for the wavelength where chlorophyll $a$ (Chl $a$) absorbs the most (430 nm; South and Whittick, 1987) using the equation:

$$I_D = I_0 * \exp(-k * z) \tag{1}$$

where $I_D$ is the irradiance at depth $z$, $I_0$ the subsurface irradiance, and $k$ the diffuse attenuation coefficient. A minor error must be assumed, since the attenuation coefficient did not take into account the shading effects by phytoplankton at the Chl $a$ maximum (located below 20 m).
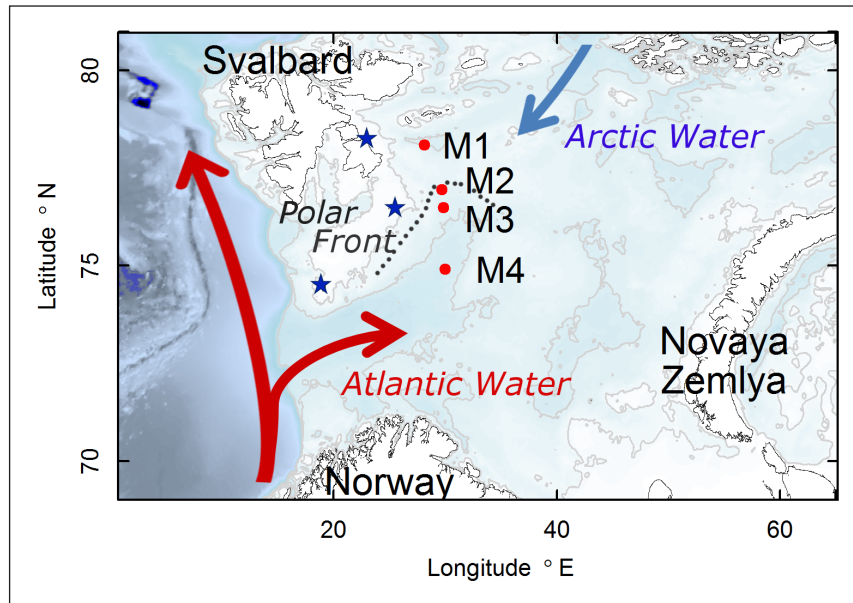
Wind data were noted in the ship's log during each operation, but due to a malfunction of the ship's wind measurement device, data are missing between 23 June (13:00 UTC) and 26 June (08:00 UTC). To interpolate these wind data, we combined our wind measurements with data from three land-based weather stations (Hopen, Bjørnøya, and Edgeøya) of the Norwegian Meteorological Institute (data available at www.yr.no).

### 2.2 Turbulence, nitrate concentrations and nitrate flux

A loosely tethered microstructure drop sonde (MSS-90 L) with a pair of PNS06 shear probes (Prandke and Stips, 1998) was used to collect sets of 2–3 profiles roughly every four hours during station work, as previously described (Sundfjord et al., 2007; Randelhoff et al., 2016). Only the set of profiles taken closest in time to the CTD and the nitrate profiles are included here. The shear profiles were processed as described in Fer (2006), where data above 8 m are discarded to avoid influence from the ship's keel.

The dissipation $\varepsilon$ (W kg$^{-1}$) was calculated using the equation given by Yamazaki and Osborn (1990):

$$\varepsilon = 7.5 \, \nu \, [(\partial u'/\partial z)^2] \tag{2}$$

Wiedmann et al: Upward nitrate flux and downward particulate organic carbon flux under contrasting situations of stratification and turbulent mixing in an Arctic shelf sea

Art. 43, page 3 of 15



**Figure 1: Map showing the Barents Sea with the sampling stations.** Hydrography in the Barents Sea is influenced by Atlantic-derived water (red arrows, entering from the southwest) and Arctic-derived water (blue arrow, entering from the northeast). The four sampling stations were in the Arctic-influenced part of the Barents Sea (M1, north of the Polar Front, indicated by the dotted line), in the region of the Polar Front (M2, M3) and in the Atlantic-influenced part (M4). The blue stars designate the land-based weather stations (from north to south: Edgeøya, Hopen and Bjørnøya). DOI: https://doi.org/10.1525/elementa.235.f1

**Table 1:** Station identity and sampling schedule. DOI: https://doi.org/10.1525/elementa.235.t1

| Station | Position | Date (2011) | Depth (m) | Ice cover | Chl $a$ max (m) | Suspended sampling[a] time (UTC) | Deployment trap array[b] time (UTC) | Deployment time (d) |
|---|---|---|---|---|---|---|---|---|
| M1 | 78.0973°N, 28.1258°E | 22 June | 278 | Very open drift ice (30%) | 31 | 16:45 | 23:30 | 0.85 |
| M2 | 76.9493°N, 29.7117°E | 24 June | 235 | Very open drift ice (20%) | 44 | 07:46 | 16:15 | 0.94 |
| M3 | 76.4910°N, 29.8630°E | 25 June | 282 | Open water | 32 | 04:34 | 21:30 | 0.82 |
| M4 | 74.9107°N, 30.0033°E | 27 June | 371 | Open water | 45 | 09:11 | 16:55 | 0.98 |

[a] sampled parameters: chlorophyll $a$ (Chl $a$), particulate organic carbon (POC) and nitrogen (PON) at 1, 5, 10, 20, 30, 40, 50, 60, 90, 120, 200 m and Chl $a$ maximum.
[b] sampled parameters: POC and PON at 40, 50, 60, 90, 120 m (and 200 m at M1 and M2).

where $\nu$ is the temperature-dependent viscosity of seawater and $\partial u'/\partial z$ represents the shear. The horizontal velocity variation $u'$ and the depth $z$ were both resolved to centimeter scale.

In a second step, we calculated the diffusivity $K$ (m² s⁻¹) following Osborn (1980) and using:

$$K = \Gamma\varepsilon/N^2 \qquad (3)$$

dividing the product of the dissipation rate $\Gamma$ (set to a typical value of 0.2; Moum, 1996) and the dissipation $\varepsilon$ by the squared Brunt-Väisälä frequency $N$. Diffusivity data were then averaged over 4-m moving intervals before being used to calculate the nitrate flux.

Continuous depth profiles of nitrate were measured with a Satlantic ISUS V3 ultraviolet spectrophotometer, integrated in the ship-borne CTD system to get simultaneous depth data from the CTD's pressure sensor. The individual nitrate sensor spectra were then processed using the manufacturer's software. The vertical profiles were first objectively adjusted to match near-surface (10 m) nitrate concentration achieved from chemical seawater analysis (procedure following Martin et al., 2010b) and then smoothed using a 10-m moving average before the gradients were obtained for the nitrate flux calculations. Even though individual nitrate measurements have an accuracy of ±2 mmol m⁻³ (Johnson and Coletti, 2002), we expect the vertical gradients to be represented more accurately by using the moving average. The nitracline is here defined as the depth layer in which the nitrate concentration rapidly increases from low surface concentrations to the (subsurface) maximum concentration (Omand and Mahadevan, 2015).

Computation of the nitrate flux $F_N$ was based on the nitrate ($N$) concentration with depth $z$ and the diffusivity ($K$), using the equation:

$$F_N = -K * (\mathrm{d}N / \mathrm{d}z) \qquad (4)$$

where here the upward nitrate flux always represents the flux from a depth layer below (e.g. 200 m – depth x) into a depth layer above (depth x – surface).

### 2.3 Nitrate uptake rates

Nitrate uptake rates are strongly dependent on the available photosynthetically active radiation (PAR). To assess this relationship, water from the surface and the subsurface Chl $a$ maximum (SCM) was collected at each station, split into ten 500 mL tissue culture flasks and each spiked with a trace amount of $^{15}$N-potassium nitrate (0.1 μM). Each set of ten flasks was placed in a separate ten-position, linear light-gradient incubator designed to minimize spectral shift (Babin et al., 1994). The incubators were illuminated by a single full-spectrum 400 W Optimarc metal-halide lamp mimicking solar irradiance. Optically neutral filters (Lee Filters) were placed in front of the incubator with the surface samples to yield measured irradiances ranging from 5 to 630 μmol quanta m$^{-2}$ s$^{-1}$. For the incubator with SCM samples, one layer of a blue filter (118 Light Blue Lee Filters Ltd.) was combined with optically-neutral filters (Lee Filters) to provide irradiances ranging from 3 to 365 μmol quanta m$^{-2}$ s$^{-1}$. Temperature was maintained at in situ levels with a chilling circulator. In order to minimize isotopic dilution and photo-acclimation to experimental conditions, the incubations were kept as short as possible (5–6 h) to ensure detection of the $^{15}$N label in particulate organic nitrogen (PON). Incubations were terminated by filtration onto 24-mm pre-combusted Whatman GF/F filters. All filters were desiccated at 60°C and stored dry for analysis ashore. An elemental analyzer (ECS 4010, Costech Analytical Technologies Inc.) coupled to a mass spectrometer (Delta V Advantage, Thermo Finnigan) was used to determine PON and its isotopic enrichment using a modified Dumas method (for details see Blais et al., 2012).

Specific nitrate uptake ($V$) was calculated using equation 3 of Collos (1987), and uptake-irradiance parameters (and standard errors on these parameters) were calculated on specific uptake data using the double exponential model of Platt et al. (1980):

$$V = V_d + V_s \left[1 - \exp\left(-\alpha E / V_s\right)\right] \left[\exp\left(-\beta E / V_s\right)\right] \qquad (5)$$

and

$$V_{max} = V_s \left[\alpha / \left(\alpha + \beta\right)\right] \left[\beta / \left(\alpha + \beta\right)\right]^{\beta/\alpha} \qquad (6)$$

where $V_d$ is the dark uptake (h$^{-1}$), $V_s$ is the theoretical maximum uptake in the absence of photoinhibition (h$^{-1}$), $V_{max}$ is the maximum observed uptake (h$^{-1}$), $E$ is the incubation irradiance (PAR, μmol quanta m$^{-2}$ s$^{-1}$), and $\alpha$ and $\beta$ [h$^{-1}$ (μmol quanta m$^{-2}$ s$^{-1}$)$^{-1}$] are the photosynthetic efficiency at low irradiance (initial slope of the relationship) and the photoinhibition parameter, respectively.

The model formulated by Platt et al. (1980) was initially developed to describe the relationship between primary production and light intensity, but Tremblay et al. (2006) and Martin et al. (2012) have shown that this approach can also be used successfully to assess nitrate uptake. Compared to other set-ups, this approach (1) allows short incubation times (minimizing bottle effects and artefacts) and (2) provides dynamic parameters, which can be used to run a simulation spanning a few days, enabling us to compare the nitrate 'demand' at the two most contrasting stations. In order to estimate nitrate uptake in a given layer, we combined the continuous record of PAR on deck with the vertical attenuation coefficient of underwater irradiances ($k$), measured at local noon, to estimate $E$ and compute equation 5 at each 1-m depth bin throughout the day. While absolute nitrate uptake would normally be obtained by multiplying equation 5 by PON, the latter was not available at a 1-m resolution. To circumvent this limitation, the specific uptake parameters were first converted into Chl $a$-specific, absolute values through multiplication by PON and division by the Chl $a$ concentration of the incubated samples (noting that concentrations of Chl $a$ and PON were well correlated during our field study; $R^2$ = 0.73 ± std dev 0.14). Uptake-irradiance parameters thus established with the surface sample were assigned to all depths in the upper mixed layer, whereas parameters established for the SCM were used at the SCM and below it. Between the base of the mixed layer and the SCM, parameters were interpolated according to the vertical gradient of nitrate concentration for $V_d$ and $V_{max}$, and according to depth for $\alpha$ and $\beta$. This procedure is justified by the fact that the nitrate concentration and depth were robust predictors of $V_{max}$ and $\alpha$, respectively, for the set of eight curves obtained for stations M1, M2, M3, and M4 at the surface and the SCM (Table S1), though we note that this procedure could not take into account possible changes in taxonomy and shade acclimation below the SCM.

For M1 and M4, the stations that we investigated in detail, absolute nitrate uptake rates (μmol N L$^{-1}$ h$^{-1}$) were then estimated for each depth bin and time of day by multiplying Chl $a$-normalized absolute N uptake by Chl $a$. The latter was estimated from post-calibrated in vivo fluorescence data from the CTD. By iterating this numerical approach, vertically integrated nitrate uptake in a given layer at M1 and M4 was averaged over five days to prevent giving too much importance to short-term conditions at the time of sampling.

### 2.4 Suspended and sedimenting biomass (Chl a, POC, PON, C/N ratio)

Suspended biomass was collected with Niskin bottles attached to the CTD rosette at 12 sampling depths between subsurface and 200 m (**Table 1**) to construct depth profiles of Chl $a$, POC, PON and the atomic C/N ratio. Collected water was gently transferred from Niskin bottles into carboys and stored cool and dark until filtration within few hours. Triplicates (50–200 mL) of each depth were vacuum-filtered onto Whatman GF/F filters (pore size 0.7 μm) and Whatman Nucleopore membrane filters (pore size 10 μm)

Wiedmann et al: Upward nitrate flux and downward particulate organic carbon flux under contrasting situations of stratification and turbulent mixing in an Arctic shelf sea

Art. 43, page 5 of 15

to achieve a size-fractionation of the Chl *a* containing material (total and >10 μm). Chl *a* was extracted in 5 mL methanol (12 h, room temperature, darkness) and the Chl *a* concentration was measured using a Turner Design 10-AU fluorometer (calibrated with Chl *a*, Sigma C6144), applying the acidification method (Holm-Hansen and Riemann, 1978). For POC and PON, triplicates (200 mL) of each sampling depth were filtered on pre-combusted Whatman GF/F filters. Larger organisms such as copepods or chaetognats were removed before the filters were frozen (–20°C) until analyses (<6 months). Analyses were carried out using a Leeman Lab CHN Elemental Analyzer (for details see Reigstad et al., 2008). A C/N ratio of 6.6 (Redfield ratio; Redfield, 1934, 1958) has traditionally been an indicator for very recently produced ("fresh") phytoplankton material, while higher ratios have been assumed to indicate more degraded biological material or material of terrestrial origin. Research during the last years, however, has shown that the C/N ratio of suspended material can vary with the physiological state of phytoplankton (e.g. nitrate depletion, as in Mei et al., 2005, and light limitation, as in Geider and La Roche, 2002) or the species composition (Fernández-Méndez et al., 2014). In addition, Frigstad et al. (2014) reported that the C/N ratio was considerably different in the Atlantic-influenced part of the Barents Sea (C/N = 6.7) and the Arctic-influenced part (C/N = 7.9). Taking this uncertainty into account, we assessed the "freshness" of the suspended biomass by a combination of microscopic cell counts and the C/N ratio.

A surface-tethered sediment trap array was deployed for 20–24 h at each of the four sampling stations (**Table 1**). Semi-Lagrangian drifting was ensured by anchoring the trap array on an ice-floe at M1 and M2. At M3 and M4 the trap array was freely drifting in open waters, but with the buoyancy located below the surface to minimize wind drift and potential pumping caused by wave action. Paired trap cylinders (KC Denmark, inner diameter 72 mm, length 450 m) were mounted at each sampling depth, determining the downward flux at 40, 50, 60, 90, and 120 m at all stations, as well as at 200 m at M1 and M2. The content of the cylinders was transferred into carboys after trap array recovery and stored cool and in darkness until filtered in triplicates (200 mL; swimmers were removed to the extent possible) and analyzed as described previously for suspended POC and PON. To be able to compare the attenuation of the POC flux at all four stations, we calculated the percentage relative to 120 m following the equation:

$$\text{Attenuation of sinking POC } (120)$$
$$= \frac{\text{strongest POC flux at station} - \text{POC flux at } 120\,m}{\text{POC flux at } 120\,m} \quad (7)$$

### 2.5 1-D residence time calculations
The upward nitrate flux and the nitrate uptake by autotrophs affect the nitrate stock in the upper water column. We conducted simple 1-D residence time calculations for M1 and M4 (**Table 2**) to investigate how

**Table 2:** Integrated nitrate stock in biologically important layers and the upward nitrate flux into them[a]. DOI: https://doi.org/10.1525/elementa.235.t2

| Station | Biologically important layer | Depth interval (m) | Integrated nitrate stock (mmol m⁻²) | Upward nitrate flux into base of layer | | Integrated nitrate uptake[b] (mmol m⁻² d⁻¹) | Time to nitrate exhaustion (d) | |
|---|---|---|---|---|---|---|---|---|
| | | | | (mmol m⁻² d⁻¹) | (% d⁻¹) | | Without upward nitrate flux | With upward nitrate flux[c] |
| M1 | Low nitrate surface layer (<0.6 mmol m⁻³) | 0–11 | 6.1 | 0.01 | 0.2 | 0.4 | 15 | 16 |
| | Mixing layer | 0–13 | 7.3 | 0.00 | 0.0 | 0.5 | 16 | 16, 45[d] |
| | Mixed layer | 0–23 | 15.7 | 0.06 | 0.4 | 1.0 | 16 | 17 |
| | Above SCM[e] layer | 0–40 | 99.8 | 0.07 | 0.1 | 14.6 | 7 | 7 |
| | Euphotic zone | 0–65 | 277.9 | 0.01 | 0.0 | 17.4 | 16 | 16 |
| M4 | Low nitrate surface layer (<0.6 mmol m⁻³) | 0–17 | 8.8 | 30.00 | 341.0 | 0.9 | 10 | _[f] |
| | Mixing layer | 0–25 | 14.4 | 5.40 | 37.5 | 1.5 | 10 | _[f], 16[g], 21[h], 25[i] |
| | Mixed layer | 0–38 | 34.2 | 0.11 | 0.3 | 3.5 | 10 | 10 |
| | Above SCM layer | 0–45 | 52.1 | 0.34 | 0.7 | 5.0 | 10 | 11 |
| | Euphotic zone | 0–45 | 52.1 | 0.34 | 0.7 | 5.0 | 10 | 11 |

[a] From shallowest to deepest layer; see section 2.4 for explanation of the calculations.
[b] 5-day mean.
[c] Nitrate upward flux as given in this table (column for upward nitrate flux into base of layer) unless specified otherwise.
[d] Nitrate upward flux 0.004 mmol m⁻² d⁻¹ for 5 days, then upward nitrate flux of 0.350 mmol m⁻² d⁻¹.
[e] Subsurface chlorophyll *a* maximum.
[f] The layer would not be replenished if assuming the upward nitrate flux in the table.
[g] Nitrate upward flux of 5.395 mmol m⁻² d⁻¹ for 1 day, then upward nitrate flux of 0.300 mmol m⁻² d⁻¹.
[h] Nitrate upward flux of 5.395 mmol m⁻² d⁻¹ for 2 days, then upward nitrate flux of 0.300 mmol m⁻² d⁻¹.
[i] Nitrate upward flux of 5.395 mmol m⁻² d⁻¹ for 3 days, then upward nitrate flux of 0.300 mmol m⁻² d⁻¹.

Art. 43, page 6 of 15

Wiedmann et al: Upward nitrate flux and downward particulate organic carbon flux under contrasting situations of stratification and turbulent mixing in an Arctic shelf sea

the integrated nitrate concentration in a certain layer of biological relevance is influenced by the nitrate uptake and the upward nitrate flux into this layer from below. The following five depth layers were investigated in detail:

1) the "low nitrate surface layer" with nitrate concentrations ≤0.6 mmol nitrate $m^{-3}$ (A limiting nitrate surface layer with <0.5 mmol nitrate $m^{-3}$ could not be investigated, because nitrate concentrations <0.5 mmol $m^{-3}$ were found only in the uppermost 5–6 m at M1. Turbulence measurements from this depth interval were omitted, however (Section 2.1), and thus no upward nitrate flux into this layer could be calculated. As an alternative, we studied the "low nitrate surface layer" defined by ≤0.6 mmol nitrate $m^{-3}$.),
2) the depth interval above the SCM,
3) the euphotic zone (irradiance >1% of the subsurface irradiance),
4) the mixed layer, and
5) the mixing layer.

By coincidence, the depth range of some layers overlapped (e.g. euphotic zone and SCM at M4), but we chose to keep both to provide a holistic picture in **Table 2**. The contribution of the upward nitrate flux to the stock (% input from below; **Table 2**) was calculated as the ratio of the upward nitrate flux into a layer to the integrated nitrate concentration in this layer. The time to nitrate exhaustion in each layer (without taking upward nitrate flux into account) equals the ratio of the integrated nitrate stock in the layer to the integrated nitrate uptake in it. To calculate the time to nitrate exhaustion with the upward nitrate flux, we started with the integrated nitrate stock in the depth layer and assumed, for each consecutive day, a constant nitrate uptake and a certain upward nitrate flux.

## 3. Results
### 3.1 Hydrography and wind
Station M1 in the northern Barents Sea was covered with very open drift ice (30%, **Table 1**). A halocline (7–23 m) structured the water column in a well-mixed, meltwater-affected, surface layer (upper 7 m: temperature $T = -1.2°C$, salinity $S = 32.9$; **Figure 2a**) and a zone below, which con-
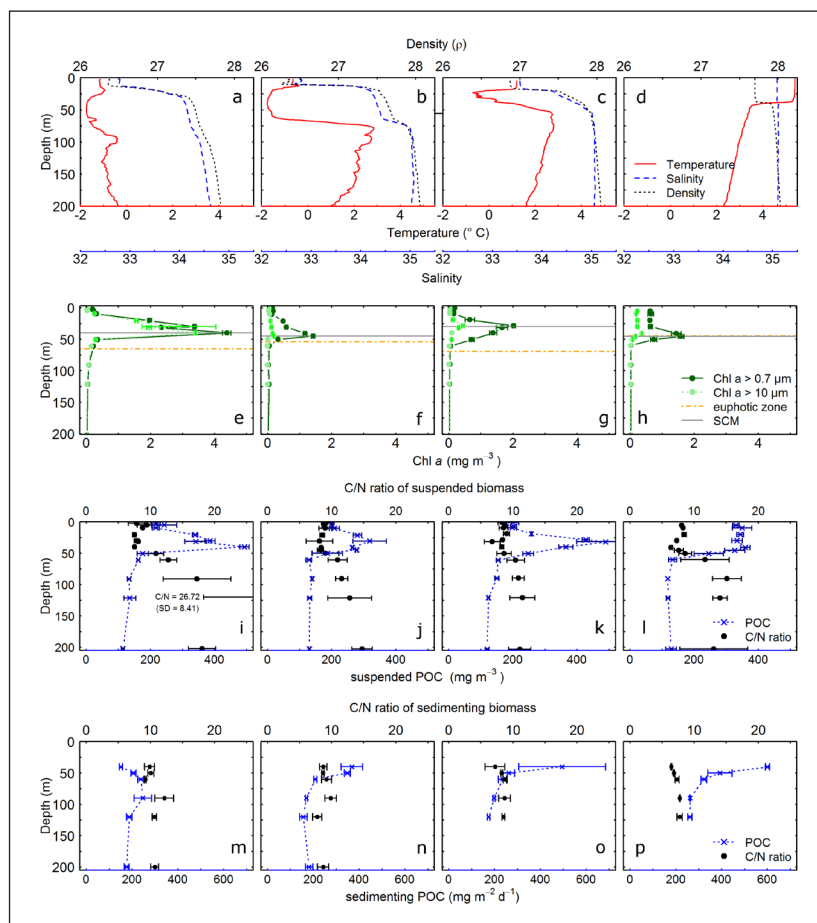


**Figure 2: Hydrography and suspended and sedimenting biomass at the sampling stations.** Hydrography with temperature (red line), salinity (blue stippled) and density (black dotted) in first row **(a, b, c, d)**. Subsurface chlorophyll *a* maximum (SCM, grey line), euphotic zone (orange stippled line) and suspended chlorophyll *a* (Chl *a*, dark green: >0.7 μm; light green: >10 μm) in second row **(e, f, g, h)**. Suspended particulate organic carbon (POC, blue crosses and blue stippled line) and atomic C/N ratio (black dots) in the third row **(i, j, k, l)** and the sedimenting POC and its atomic C/N ratio in the fourth row **(m, n, o, p)**. Left column: station M1, second column from left: M2, second column from right: M3, right column: station M4. DOI: https://doi.org/10.1525/elementa.235.f2

Wiedmann et al: Upward nitrate flux and downward particulate organic carbon flux under contrasting situations of stratification and turbulent mixing in an Arctic shelf sea

Art. 43, page 7 of 15

sisted of Arctic-originating water gradually mixed with Atlantic water at depth (25–200 m: $T < 0°C$, $S = 34.0$–$34.7$).

Station M2 was located at the Polar Front in very open drift ice (20%; **Table 1**). In this area, colder and fresher Arctic-derived water masses tend to cover warmer and more saline Atlantic-derived waters (Loeng, 1991) which was also observed during our study (**Figure 2b**). A well-mixed meltwater layer (0–15 m: $T < 0.0°C$, $S = 32.6$) was separated by a strong halocline (15–20 m) from the lower part of the water column, which was influenced, increasingly with depth, by Atlantic water (200 m: $T = 0.9°C$, $S = 35.0$).

Station M3 was in ice-free waters. Its well-mixed surface layer (0–16 m) showed an influence of recent ice melt ($S < 33.6$; **Figure 2c**) and atmospheric warming (>1°C). Arctic-derived water masses prevailed at 20–30 m ($T < 0°C$, $S < 34.5$), but warmer and more saline water was found below 50 m ($T > 1.6°C$, $S > 35.0$). This layering indicated that M3 was also situated in the Polar Front.

Station M4 was located in the ice-free, Atlantic-influenced, southern Barents Sea. The stratification was relatively weak and dominated by a temperature gradient (**Figure 2d**). Water masses were characterized by $T > 5.0°C$ (salinity of 35.09) above the thermocline, but $T = 3.5°C$ below it (40 m), and gradually decreasing with depth (200 m: $T = 2.3°C$). The salinity was fairly constant below the thermocline ($S = 35.10$–$35.13$).

A fresh to strong breeze was recorded at M1 (9.5–13.3 m s$^{-1}$) and M3 (9.3–13.5 m s$^{-1}$), while a moderate to fresh breeze prevailed at M4 (5.5–10.9 m s$^{-1}$; **Figure 3**). Wind data from M2 are lacking due to the malfunction of our vessel's wind current meter, but land-based permanent weather stations in the area (Bjørnøya, Hopen and Edgeøya; **Figure 1**) recorded a wind speed

of 3–10 m s$^{-1}$ during this period. Following Coelingh et al. (1996), who concluded that the wind speed in the southern North Sea tended to be higher at sea-based stations compared to coastal ones, we presume that the wind speed at M2 was in the range of wind speed encountered at M1 and M3.

### 3.2 Euphotic zone and suspended biological parameters (size fractionated Chl a, POC, C/N ratio)

At station M1 the base of the euphotic zone (1% irradiance of surface irradiance at 430 nm) was at 65 m (**Figure 2e**). The SCM at 40 m had the highest Chl $a$ concentration of the present study (4.4 mg Chl $a$ m$^{-3}$). The Chl $a$ was dominated by small cells in the upper 5 m (approximately 90% < 10 µm; **Figure 2e**), but larger cells prevailed between 10 and 120 m (66–90% > 10 µm; **Figure 2e**). The most abundant taxa were the phytoplankton genera *Chaetoceros, Thalassiosira* and *Phaeocystis* (Wiedmann et al., 2014: $265 \times 10^3$ cells L$^{-1}$, $156 \times 10^3$ cells L$^{-1}$, and $107 \times 10^3$ cells L$^{-1}$, respectively), and despite the presence of sea ice, no ice algae were found. The Chl $a$ peak was well correlated to the depth distribution of suspended POC and PON ($R^2 = 0.91$ and $0.86$), and the C/N ratio of 7.5–9.5 suggested little to moderately degraded suspended biomass down to 50 m (**Figure 2i**), which was confirmed by microscopic cell counts (healthy cells and few resting spores).

At M2 the euphotic zone reached to a depth of 54 m (**Figure 2f**) and the SCM was found at 44 m (1.5 mg Chl $a$ m$^{-3}$). The microalgae community was dominated by small phytoplankton (50–80% < 10 µm; **Figure 2f**) down to 200 m, and the species *Phaeocystis pouchetii* ($274 \times 10^3$ cells L$^{-1}$; Wiedmann et al., 2014) prevailed, though larger pelagic taxa were also found
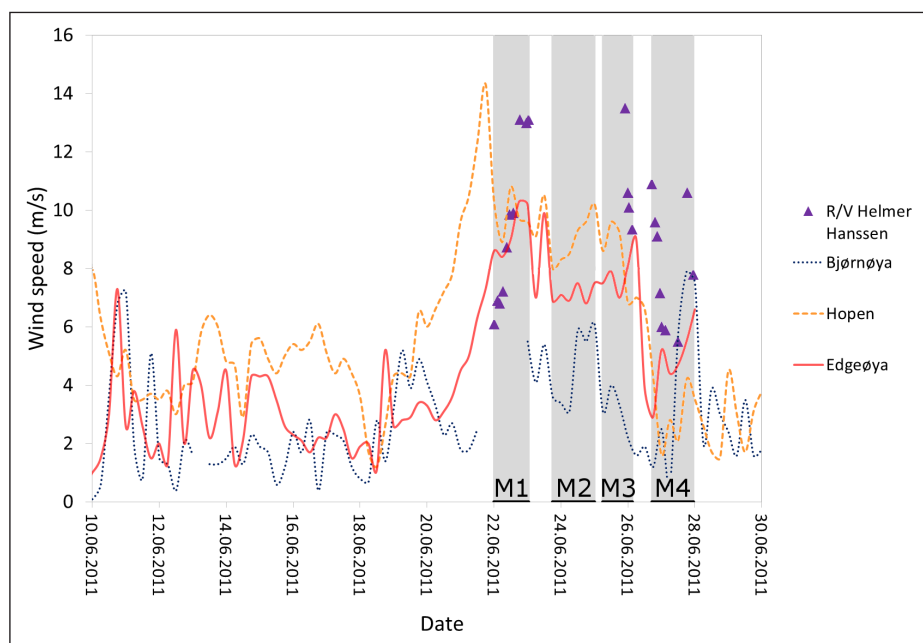


**Figure 3: Wind speed measurements recorded on land-based stations and on the research vessel.** Wind data from the land-based measurements stations on Bjørnøya (blue dotted line), Hopen (orange stippled line) and Edgeøya (red line) between 10 June 2011 and 30 June 2011 and the wind speed recordings on the R/V *Helmer Hanssen* (violet triangles). Grey shaded areas indicate the time spent at the four sampling stations (M1–M4). DOI: https://doi.org/10.1525/elementa.235.f3

Art. 43, page 8 of 15

Wiedmann et al: Upward nitrate flux and downward particulate organic carbon flux under contrasting situations of stratification and turbulent mixing in an Arctic shelf sea

(*Chaetoceros* sp., 3700 cells L$^{-1}$, and *Thalassiosira* sp., 30 × 10$^3$ cells L$^{-1}$). The Chl *a* depth profile correlated moderately with the POC and PON depth distribution (R$^2$ = 0.56 and 0.54, respectively) and the C/N ratio of 8.1–9.2 (top 50 m) indicated that the suspended biomass was in a similar state of "freshness" as at M1 (**Figure 2j**).

The deepest euphotic zone (approximately 70 m) and the shallowest SCM (30 m: 2.0 mg m$^{-3}$; **Figure 2g**) was observed at station M3. No cell counts are available for this station, but M3 was also dominated by small cells (70–90%) and the Chl *a* depth profile correlated well with the POC and PON depth distribution (R$^2$ = 0.93 and 0.82, respectively). Apart from the 32 m sample directly under the SCM (C/N = 6.8), the C/N range at M3 was similar to the range observed at M2 and M1 (**Figure 2k**).

At station M4, the base of the euphotic zone coincided with the SCM (both at 45 m; Chl *a* concentration: 1.6 mg m$^{-3}$; **Figure 2h**). The phytoplankton taxon *Phaeocystis* clearly dominated (1.810 × 10$^6$ cells L$^{-1}$; Wiedmann et al., 2014), and only few large cells (*Thalassiosira* sp. 4050 cells L$^{-1}$) were found. In contrast to the Chl *a* depth distribution, the suspended POC was rather evenly distributed in the upper 40 m (**Figure 2h** and **l**) and thus the two parameters were only moderately correlated (R$^2$ = 0.64). A better correlation was found between the Chl *a* and the PON depth profile (R$^2$ = 0.73). The C/N ratio of the suspended biomass in the top 50 m (consisting almost exclusively of single cells of *Phaeocystis pouchetii*) was somewhat lower than at the previous stations (C/N = 6.4–8.6; **Figure 2l**).

Based on the integrated nitrate concentrations (**Figure 4a, b**; M2 and M3 not shown), the Chl *a* concentration, the relative abundance of small cells, and the composition of phytoplankton and zooplankton (C. Svensen, unpublished data), the bloom stage was determined at our four sampling stations. We classified them as a late peak bloom stage (M1), a late bloom stage (M2, M3) and post-bloom stage (M4), respectively. The term "late peak bloom" (M1) may not be very common, but we use it here to describe that M1 was in a late stage of a peak bloom, because we found in the surface waters 1) low nitrate concentrations, 2) high Chl *a* concentration, dominated by large phytoplankton at ≥10 m), yet 3) an abundant zooplankton community, mainly consisting of copepod eggs and nauplii (C. Svensen, unpublished data).

### 3.3 Nitrate concentration and nitrate flux at M1 and M4

The suspended biological variables and hydrography, as well as the data on vertical export, implied a gradual change from north to south, which we used as a space-for-time substitution to investigate the impact of the upward nitrate flux at the two most contrasting
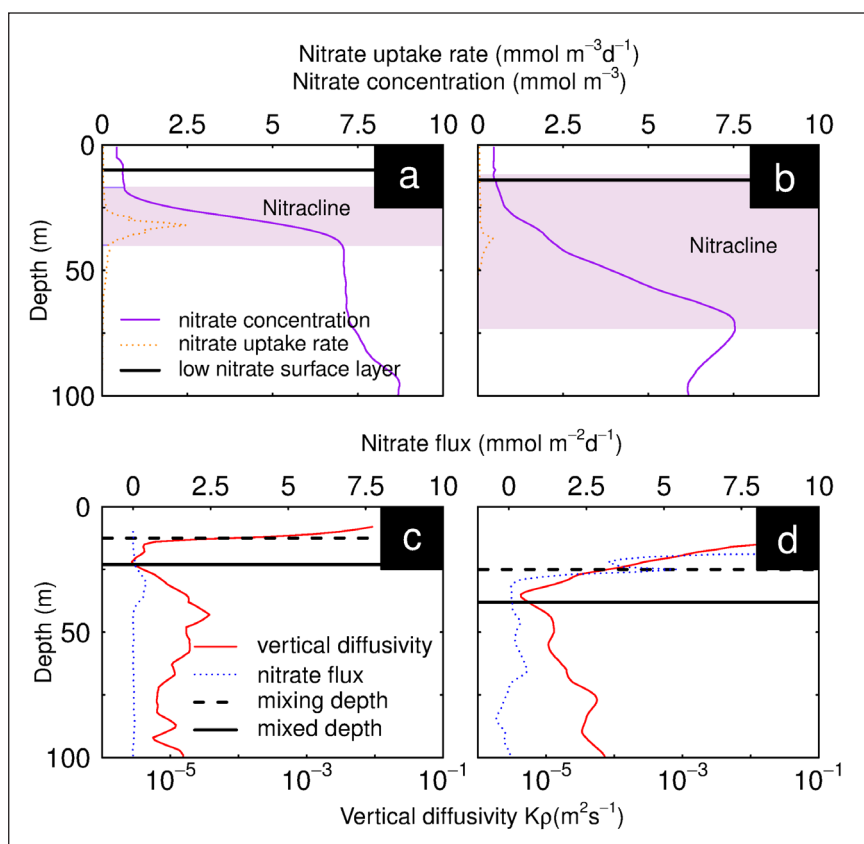


**Figure 4: Nitrate concentration, nitrate uptake rates and mixing depth at the two most contrasting stations.** Nitrate concentrations (purple line), nitrate uptake rates (orange dotted line) and nitracline (purple shaded field) at station M1 **(a)** and M4 **(b)** in the upper row. Vertical diffusivity (red line) and the upward nitrate flux (blue dotted line) in the lower row **(c, d)**. The black lines indicate the layers used in the 1-D residence time calculation (a, b: solid line, low nitrate surface layer with a nitrate concentration ≤0.6 mmol nitrate m$^{-3}$; c, d: dashed line, mixing depth; solid line, mixed depth). DOI: https://doi.org/10.1525/elementa.235.f4

Wiedmann et al: Upward nitrate flux and downward particulate organic carbon flux under contrasting situations of stratification and turbulent mixing in an Arctic shelf sea

Art. 43, page 9 of 15

situations M1 and M4. At M1, the nitrate concentration was low in the upper 11 m (<0.6 mmol m$^{-3}$, **Figure 4a**) and, with surface-enhanced mixing protruding only to 13 m (mixing depth; **Figure 4c**), a weak upward nitrate flux of 0.01 mmol nitrate m$^{-2}$ d$^{-1}$ was estimated into the low nitrate surface layer (0–11 m; **Figure 4a, Table 2**). Because of the strong stratification of the water column (**Figure 2a**), the upward nitrate flux into the upper part of the nitracline (20–25 m) was also low (**Figure 4a, c**). However, between 25 m and nearly 40 m, the stratification was weaker (**Figure 2a**), and the upward nitrate flux was 0.1–0.4 mmol m$^{-2}$ d$^{-1}$ (**Figure 4c**). Below 40 m, a combination of declining vertical diffusivity and a vertically rather stable nitrate concentration resulted in a weak upward nitrate flux (<0.1 mmol m$^{-2}$ d$^{-1}$; **Figure 4c**). Overall, the nitrate flux contributed little to the nitrate stock in our five depth layers, which we investigated in detail (**Table 2**).

At M4, the nitrate concentration increased from the surface (1 m: <0.5 mmol nitrate m$^{-3}$) to a subsurface maximum at approximately 73 m (7.54 mmol nitrate m$^{-3}$; **Figure 4b**). The minor decline in nitrate concentration below the subsurface maximum values (**Figure 4b**) likely reflects differences in advection history at the different subsurface depths. The enhanced diffusivity (>10$^{-4}$ m$^2$ d$^{-1}$) in the uppermost 25 m resulted in an upward nitrate flux of 30.0 mmol nitrate m$^{-2}$ d$^{-1}$ into the low nitrate surface layer and 5.4 mmol nitrate m$^{-2}$ d$^{-1}$ into the mixing layer (**Figure 4d**, **Table 2**). This flux replenished the nitrate stock in the low nitrate surface layer (0–17 m) and the mixing layer (0–25 m) by approximately 341% d$^{-1}$ and 38% d$^{-1}$ (**Table 2**). The contribution of the upward nitrate flux to the nitrate stock in the other layers at M4 was <1%, which still exceeded the contribution into the respective layers at M1.

### 3.4 Nitrate uptake rates and time to nitrate exhaustion

The nitrate uptake rate peaked at 32 m at M1 (2.5 mmol nitrate m$^{-3}$ d$^{-1}$; **Figure 4a**), and at 37 m at M4 (0.4 mmol nitrate m$^{-3}$ d$^{-1}$; **Figure 4b**). By using 1-D residence time calculations, we aimed to assess changes in the integrated nitrate concentration by nitrate uptake and the upward nitrate flux in our five layers. At M1, the nitrate concentration declined in the five depth layers, whether or not the upward nitrate flux into this layer was taken into account (**Table 2**). The nitrate flux was too weak to compensate for the nitrate uptake, and including it into our 1-D calculations prolonged the time to nitrate exhaustion by only one day at maximum. The 1-D calculations for the above SCM layer, the euphotic zone and the mixed layer at M4 gave the same result (**Table 2**). Considerably different results, however, were obtained for the low nitrate surface layer and the mixing layer at M4. Because of the intense upward nitrate flux, which exceeded the nitrate uptake rate, the nitrate stock could be replenished at M4. We conducted additional calculations for the mixing layer at M4 (**Table 2**), because Sakshaug and Slagstad (1992) suggested that strong wind events may occur at 10-day intervals in the southern Barents Sea, causing episodic periods

of enhanced mixing. We recorded wind speed >12 m s$^{-1}$ at M3, and thus presumed that a strong wind event had also occurred at M4 prior to our arrival there (**Figure 3**). This event would have likely induced vertical mixing processes and resulted in high diffusivity and strong upward nitrate flux, which we observed at M4 (**Figure 4d**). We aimed to transfer this situation into our 1-D calculation by using a high upward nitrate flux into the mixing layer for 1–3 days, followed by a weaker upward nitrate flux of 0.30 mmol nitrate m$^{-2}$ d$^{-1}$. The latter equals an average flux at 50–70 m, a depth interval not influenced by surface mixing processes. Our 1-D residence time calculation suggested that, for a situation of strong mixing (1, 2, or 3 days) followed by a period of relaxation, the integrated nitrate concentration in the mixing layer was replenished considerably and the period to nitrate depletion in the mixing layer was prolonged to 16, 21 or 25 days (**Table 2**).

### 3.5 Characterization of the vertical flux (POC, C/N ratio)

The downward POC flux (at 120 m) was higher at M4 (261 mg POC m$^{-2}$) than at the other stations (156–187 mg POC m$^{-2}$ d$^{-1}$; **Figure 2m–p**), and the attenuation of the flux was weakest at M1 (M1: 22%; M2–M4: 58–65%). The C/N ratio of the sinking biomass was highest at the northernmost station M1, intermediate at M2 and M3 and lowest at M4 (**Figure 2m–p**). The composition of the sinking material was assessed in a previous study (Wiedmann et al., 2014) and showed that diatom colonies contributed most to the sinking biomass at M1. The sinking biomass at M2 was a mixture of diatoms, fecal pellets and unidentified matter, while it was dominated by fecal pellets at M4. No data are available from M3.

## 4. Discussion
### 4.1 Impact of water column stratification and vertical turbulent mixing on the upward nitrate flux

In marine ecosystems, the nitrate flux is commonly oriented upwards (Mann and Lazier, 2006), and the strength of this flux can vary considerably. Strongly stratified waters hamper it (Moum, 1996; Osborn, 1980), while wind-induced vertical mixing processes such as water shear, waves, Ekman pumping, frontal and eddy-induced upwelling (Omand and Mahadevan, 2015) can promote it, because these processes break down the stratification.

At station M1 in the northern Barents Sea, a combination of a moderate halocline and the presence of drift ice apparently hindered deep turbulent mixing. This hindering resulted in a low upward nitrate flux (<0.04 mmol nitrate m$^{-2}$ d$^{-1}$) into the five layers, which we investigated in detail in our 1-D residence time calculations (**Table 2**). The intensity of the upward nitrate flux at M1 was similar to previous reports from 1) the stratified, partly ice-covered, northern Barents Seas (upward nitrate flux into the upper mixed layer during a summer ice edge bloom: 0.14 mmol nitrate m$^{-2}$ d$^{-1}$; Sundfjord et al., 2007), 2) drift ice-covered waters northwest of Svalbard (May and August: nitrate flux of 0.2–0.3 mmol nitrate m$^{-2}$ d$^{-1}$; Randelhoff et al., 2016), 3) the ice-free, northeast Atlantic subpolar gyre (upward nitrate flux into the upper mixed

Art. 43, page 10 of 15

Wiedmann et al: Upward nitrate flux and downward particulate organic carbon flux under contrasting situations of stratification and turbulent mixing in an Arctic shelf sea

layer during summer: 0.02–0.60 mmol nitrate $m^{-2}$ $d^{-1}$; Painter et al., 2014), and 4) the Porcupine Abyssal Plain, NE Atlantic (upward nitrate flux into the euphotic zone during a weakly stratified summer situation: 0.09 mmol nitrate $m^{-2}$ $d^{-1}$; Martin et al., 2010a).

In contrast, the ice-free, weakly stratified waters at M4 in the southern Barents Sea were more prone to wind-induced mixing, and the upward nitrate flux into the base of the mixing layer exceeded the one at M1 by up to two orders of magnitude (>5 mmol $m^{-2}$ $d^{-1}$ into the base of the mixing layer; **Table 2**, **Figure 4c, d**). Comparatively high fluxes have been reported previously, into the base of the upper mixed layer in the southern Barents Sea during July (Sundfjord et al., 2007) and into the base of the SCM in the tidally mixed Celtic Sea during summer (Sharples et al., 2007). However, these high upward nitrate fluxes diverge from the common understanding of nitrate replenishment in the Arctic Ocean and sub-Arctic seas. Convective winter mixing is usually assumed to be the major driver of the upward nutrient flux and replenishment of the nitrate concentrations in the surface layers (Louanchi and Najjar, 2001), because thermal and meltwater stratification tends to hamper deep vertical mixing during summer (Martin et al., 2010a; Bourgault et al. 2011; Painter et al., 2014; Randelhoff et al. 2016).

Nonetheless, we consider our result of high upward nitrate flux in the southern Barents Sea during early summer as reliable, because a combination of factors seemed to facilitate the flux in this area then. The stratification in the southern, ice-free Barents Sea is not influenced by sea ice melt water, and this shelf sea, due to its location far north, is less exposed to atmospheric warming than shelf seas further south; thus, a weakly stratified water column can be found during late spring and early summer. Previous studies suggest that episodic wind events have a major effect on the southern Barents Sea (Sakshaug and Slagstad, 1992; Le Fouest et al., 2011), and a wind-mixed layer of 50–100 m depth during May has been proposed (Slagstad and McClimans, 2005). In combination with the nitracline being located at 20–70 m (Reigstad et al., 2002; Hodal et al., 2008), an intense upward nitrate flux, as observed at our station M4, is a likely event. As nitrate entrainment by a storm during a post-bloom situation has also been reported from the Bering Sea (Sambrotto et al., 1986), we hypothesize that a strong upward nitrate flux during a post-bloom situation may be a more wide-spread phenomenon in Arctic shelf seas than previously realized. More research on this phenomenon is needed.

### 4.2 Factors impacting the nitrate stock in the upper water column

The spring phytoplankton bloom at high latitudes is commonly assumed to cause a decline in the nitrate surface concentration and a deepening of the nitracline. Our observations during a late peak bloom, a late bloom and a post-bloom situation in the Barents Sea generally corresponded with this pattern. A minor modification was observed in the form of a subsurface nitrate peak at 70 m at station M4, but we assume this peak was linked to advection of nutrient-rich Atlantic water (Torres-Valdés et al.,

2013). Similar impacts on the nitrate depth profile have been reported from the Japan Sea and open oceanic sites (Kaplunenko et al., 2013; Omand and Mahadevan, 2015); such subsurface peaks do not contradict the general pattern of a nitrate decline during the spring phytoplankton bloom.

In our 1-D residence time calculation we investigated how the upward nitrate flux and the nitrate uptake modified the nitrate stock in five different layers of biological relevance at M1 and M4. These calculations have some limitations. First, the upward nitrate fluxes are based on few turbulence measurements and nitrate depth profiles; they represent only a snap-shot of the situation in the water column. Accordingly, a higher upward nitrate flux can occur in shallower waters than at greater depth (e.g. M4, 25 m: 5.40 mmol nitrate $m^{-2}$ $d^{-1}$ vs. M4, 45 m: 0.34 mmol nitrate $m^{-2}$ $d^{-1}$), but this situation can only be assumed to be sustainable for hours to few days. Second, the nitrate uptake rates represent also only snap-shot measurements because they were based on short incubations to minimize bottle effects and artefacts, but we extrapolated the uptake rates with a model, thus giving a reasonable estimate for a period of several days. Third, a potential impact of shallow water nitrification has not been included in our 1-D calculations, because relevant data for the Barents Sea were not available. In the northern Bering Sea and southern Chukchi Sea, however, Shiozaki et al. (2016) reported only a minor impact of nitrate production via nitrification, which contributed <5% to nitrate assimilation.

Given these limitations, our 1-D calculations nevertheless illustrate a potentially important set of scenarios for the Barents Sea. At M1, mixing processes were hampered by drift ice and a moderate stratification. This hampering resulted in a minor upward nitrate flux, which contributed very little to the nitrate standing stock in the layers, which we investigated in detail (**Table 2**). Similarly low rates of daily nitrate injections have been observed in the subpolar Atlantic Ocean gyre (Painter et al., 2014). In an additional calculation example (see last column of **Table 2**), we aimed to reproduce the situation of a northwards moving marginal ice zone, because ice maps from the Norwegian Meteorological Institute (www.polarview.met.no) indicate this development subsequent to our work at station M1. However, using a stronger upward nitrate flux (0.350 mmol $m^{-2}$ $d^{-1}$) only prolonged the time to nitrate depletion at M1 (**Table 2**), because the upward nitrate flux could not counterbalance the nitrate uptake rates. Thus, the situation at M1 agreed well with the common understanding of a constant decline of the nitrate surface concentration during the spring phytoplankton bloom.

At M4, the situation was different. The upward nitrate flux into the mixing layer and the low nitrogen surface layer was high enough to replenish the nitrate concentration in these layers. Our 1-D calculation suggested that this replenishment occurred even when we mirrored the pattern of 1–3 days of deep mixing (strong upward nitrate flux of >5 mmol $m^{-2}$ $d^{-1}$) followed by weak mixing (resulting in a weak upward nitrate flux). Our simple 1-D calculations thus point to an interesting concept of

Wiedmann et al: Upward nitrate flux and downward particulate organic carbon flux under contrasting situations of stratification and turbulent mixing in an Arctic shelf sea

Art. 43, page 11 of 15

two possible scenarios: a constant decline of the surface nitrate concentration obviously takes place in many high latitude regions during the spring phytoplankton bloom, but there may also be areas where an episodic replenishment of surface nitrate concentration occurs during late spring and early summer.

### 4.3 Impact of water column stratification and turbulent mixing on the downward POC flux

The intensity of the downward POC flux reflects the hydrographical situation and the ecological interactions of the plankton in the upper water column. High POC sedimentation events tend to occur when a temporal, weak coupling of primary production and grazer activity allows sinking of the produced biomass.

This situation has been suggested to occur during the ice edge phytoplankton bloom in the Barents Sea (Sakshaug et al., 1991, 2009; Wassmann and Reigstad, 2011), and our study confirms that. The downward POC flux we encountered at station M1 was comparable to previous measured exports in this region during spring (Andreassen and Wassmann, 1998; Coppola et al., 2002; Olli et al., 2002; Reigstad et al., 2008). The high Chl $a$: POC ratio and the cell counts suggest that suspended autotrophs were the prevailing form of POC in the water column, while aggregates of large diatoms (>10 μm) have been identified as the prevailing vehicle of vertically exported biomass to ≤60 m at M1 (Wiedmann et al., 2014). These aggregates can sink a few hundred meters per day, depending on species and physiological stage (Bienfang et al., 1982; Iversen and Ploug, 2013), and as mesozooplankton abundances were low at M1 (Wiedmann et al., 2014; C. Svensen, unpublished data), a weak attenuation of the sinking biomass occurred at this station in the northern Barents Sea.

Despite the common conception of a post bloom situation being associated with a minor POC sedimentation (Sakshaug et al, 2009), we found a stronger downward POC flux during the post bloom situation at M4 than during the late peak bloom at M1 (**Figure 2m, p**). Similarly high downward POC fluxes have been observed previously in the southern Barents Sea during late spring and early summer (Olli et al., 2002: in July, downward POC flux up to 400 mg POC m$^{-2}$ d$^{-1}$; Reigstad et al., 2008: in late May, 400–750 mg POC m$^{-2}$ d$^{-1}$ at 40–200 m), but the underlying mechanisms have not been fully understood.

During our study, single cells of *Phaeocystis pouchetii* (5 μm diameter) were highly abundant at M4 (Wiedmann et al., 2014). They have a low sinking velocity, but may contribute to the downward POC flux when down-mixing occurs (Reigstad and Wassmann, 2007). Because we found deep vertical mixing at M4 (**Figure 4d**), and a low C/N ratio of the sedimenting material (C/N = 6.4–7.7; **Figure 2l**) suggests a fast downward transport of recently produced biomass, we presume that down-mixing of *Phaeocystis* cells occurred at M4. Further, the mesozooplankton abundance increased during our field study from north to south (C. Svensen, unpublished data), so that an intense top-down control can be assumed at M4. Such top-down control may at a first seem to contradict the moderate biomass attenuation and strong downward POC flux observed at

M4. However, pulsed nitrate supply can stimulate primary production (southeastern Bering Sea; Sambrotto et al., 1986), which in turn may enhance feeding rates of copepods and result in the production of larger fecal pellets (Turner and Ferrante, 1979, and references therein; Wexels Riser et al., 2007). Fecal pellets have been observed frequently in the gel traps at M4 (Wiedmann et al., 2014) and, as they have a considerable sinking velocity (5–220 m d$^{-1}$; Turner, 2002), they may contribute to a fast transport from surface layers to depth. Thus, the strong downward POC flux we found at M4 may be a result of intense grazing and repackaging of slowly sinking biomass into rapidly sinking pellets. Emerging from this study are two scenarios for strong downward POC flux: one associated with the flux of large diatoms during a late peak bloom situation, and another associated with a post-bloom situation in deep mixed waters, where down-mixing of small, slowly-sinking phytoplankton cells and fast-sinking fecal pellets help to explain minor biomass attenuation in the surface layers.

## 5. Conclusion

During a field study with four stations, we observed a gradual change in the hydrography and phytoplankton bloom stage in the Barents Sea, an Arctic shelf sea. In the moderately stratified water column in the northern Barents Sea a late peak bloom prevailed, while a late bloom was found in the stratified waters of the Polar Front and a post-bloom situation in the deep-mixed waters of the southern Barents Sea. We used this space-for-time substitution to investigate the northernmost (late peak bloom) and southernmost (post bloom) station in detail as they represented the most contrasting situations. A weak upward nitrate flux characterized the stratified waters in the marginal ice zone in the north, where the flux could not counterbalance the nitrate uptake rate and our 1-D residence time calculation implied a constant decline of the nitrate concentration in the surface layers (<65 m). In contrast, a substantial upward nitrate flux was found into the surface layers (<23 m) in the Atlantic-influenced, ice-free waters of the southern Barents Sea, where the 1-D calculations suggested that the nitrate concentrations in the layers were replenished. Though a high downward POC flux is commonly associated with a peak phytoplankton bloom stage, we found a higher downward POC flux during the post-bloom situation of the southern Barents Sea compared to the late peak bloom stage in the northern Barents Sea. We suggest that the intense upward nitrate flux during the post-bloom situation stimulated the pelagic system and that a combination of downward mixed phytoplankton cells and fast-sinking fecal pellets enhanced the POC export. From the perspective of amplified climate warming in the Arctic, we see an urgent need for further investigation of the effect of deep-mixing events on the downward POC flux in ice-free, weakly stratified Arctic shelf regions with a shallow nitracline. The results of such studies will help to improve our understanding of the food supply for benthic ecosystems and bottom-associated fish stocks as well as the potential for carbon sequestration in future, ice-free Arctic regions.

Art. 43, page 12 of 15

Wiedmann et al: Upward nitrate flux and downward particulate organic carbon flux under contrasting situations of stratification and turbulent mixing in an Arctic shelf sea

## Data Accessibility Statement

All data are included in the manuscript or were previously published as Open Access (Wiedmann et al., 2014).

## Supplemental File

The supplemental file for this article can be found as follows:

- **Table S1.** Parameters used in the calculation of nitrate uptake. DOI: https://doi.org/10.1525/elementa.235.s1

## Competing interests

The authors have no competing interests to declare.

## Author contribution

- Contributed to conception and design: IW, JET, AS, MR
- Contributed to acquisition of data: IW, JET, AS, MR
- Contributed to analysis and interpretation of data: IW, JET, AS, MR
- Drafted and/or revised the article: IW, JET, AS, MR
- Approved the submitted version for publication: IW, JET, AS, MR

## References

**Andreassen, IJ** and **Wassmann, P** 1998 Vertical flux of phytoplankton and particulate biogenic matter in the marginal ice zone of the Barents Sea in May 1993. *Mar Ecol Prog Ser* **170**: 1–14. DOI: https://doi.org/10.3354/meps170001

**Arrigo, KR** and **van Dijken, GL** 2015 Continued increases in Arctic Ocean primary production. *Prog Oceanogr* **136**: 60–70. DOI: https://doi.org/10.1016/j.pocean.2015.05.002

**Babin, M, Morel, A** and **Gagnon, R** 1994 An incubator designed for extensive and sensitive measurements of phytoplankton photosynthetic parameters. *Limnol Oceanogr* **39**(3): 694–702. DOI: https://doi.org/10.4319/lo.1994.39.3.0694

**Bienfang, PK** 1981 Sinking rates of heterogeneous, temperate phytoplankton populations. *J Plankton Res* **3**(2): 235–253. DOI: https://doi.org/10.1093/plankt/3.2.235

**Bienfang, PK, Harrison, PJ** and **Quarmby, LM** 1982 Sinking rate response to depletion of nitrate, phosphate and silicate in four marine diatoms. *Mar Biol* **67**(3): 295–302. DOI: https://doi.org/10.1007/BF00397670

**Blais, M, Tremblay, J-É, Jungblut, AD, Gagnon, J, Martin, J,** et al. 2012 Nitrogen fixation and identification of potential diazotrophs in the Canadian Arctic. *Global Biogeochem Cy* **26**(3): GB3022. DOI: https://doi.org/10.1029/2011GB004096

**Bourgault, D, Hamel, C, Cyr, F, Tremblay, JÉ, Galbraith, PS,** et al. 2011 Turbulent nitrate fluxes in the Amundsen Gulf during ice-covered conditions. *Geophys Res Lett* **38**(15): L15602. DOI: https://doi.org/10.1029/2011GL047936

**Brainerd, KE** and **Gregg, MC** 1995 Surface mixed and mixing layer depths. *Deep-Sea Res I* **42**(9): 1521–1543. DOI: https://doi.org/10.1016/0967-0637(95)00068-H

**Carmack, E** and **McLaughlin, F** 2011 Towards recognition of physical and geochemical change in Subarctic and Arctic Seas. *Prog Oceanogr* **90**(1–4): 90–104. DOI: https://doi.org/10.1016/j.pocean.2011.02.007

**Carmack, E** and **Wassmann, P** 2006 Food webs and physical–biological coupling on pan-Arctic shelves: Unifying concepts and comprehensive perspectives. *Prog Oceanogr* **71**(2–4): 446–477. DOI: https://doi.org/10.1016/j.pocean.2006.10.004

**Coelingh, JP, van Wijk, AJM** and **Holtslag, AAM** 1996 Analysis of wind speed observations over the North Sea. *J Wind Eng Ind Aerodyn* **61**(1): 51–69. DOI: https://doi.org/10.1016/0167-6105(96)00043-8

**Collos, Y** 1987 Calculations of $^{15}$N uptake rates by phytoplankton assimilating one or several nitrogen sources. *Int J Radiat Appl Instrum Part A* **38**(4): 275–282. DOI: https://doi.org/10.1016/0883-2889(87)90038-4

**Coppola, L, Roy-Barman, M, Wassmann, P, Mulsow, S** and **Jeandel, C** 2002 Calibration of sediment traps and particulate organic carbon export using $^{234}$Th in the Barents Sea. *Mar Chem* **80**(1): 11–26. DOI: https://doi.org/10.1016/S0304-4203(02)00071-3

**Eppley, RW, Holmes, RW** and **Strickland, JDH** 1967 Sinking rates of marine phytoplankton measured with a fluorometer. *J Exp Mar Biol Ecol* **1**(2): 191–208. DOI: https://doi.org/10.1016/0022-0981(67)90014-7

**Falk-Petersen, S, Pavlov, V, Berge, J, Cottier, F, Kovacs, K,** et al. 2015 At the rainbow's end: high productivity fueled by winter upwelling along an Arctic shelf. *Polar Biol* **38**(1): 5–11. DOI: https://doi.org/10.1007/s00300-014-1482-1

**Fer, I** 2006 Scaling turbulent dissipation in an Arctic fjord. *Deep-Sea Res I* **53**(1–2): 77–95. DOI: https://doi.org/10.1016/j.dsr2.2006.01.003

**Fernández-Méndez, M, Wenzhöfer, F, Peeken, I, Sørensen, HL, Glud, RN, Boetius, A** 2014 Composition, Buoyancy Regulation and Fate of Ice Algal Aggregates in the Central Arctic Ocean. *PLoS ONE* **9**(9): e107452. DOI: https://doi.org/10.1371/journal.pone.0107452

Wiedmann et al: Upward nitrate flux and downward particulate organic carbon flux under contrasting situations of stratification and turbulent mixing in an Arctic shelf sea

Art. 43, page 13 of 15

**Forest, A, Babin, M, Stemmann, L, Picheral, M, Sampei, M,** et al. 2013 Ecosystem function and particle flux dynamics across the Mackenzie Shelf (Beaufort Sea, Arctic Ocean): an integrative analysis of spatial variability and biophysical forcings. *Biogeosciences* **10**(5): 2833–2866. DOI: https://doi.org/10.5194/bg-10-2833-2013

**Franks, PJS** 2015 Has Sverdrup's critical depth hypothesis been tested? Mixed layers vs. turbulent layers. *ICES J Mar Sci* **72**(6): 1897–1907. DOI: https://doi.org/10.1093/icesjms/fsu175

**Frigstad, H, Andersen, T, Bellerby, RGJ, Silyakova, A** and **Hessen, DO** 2014 Variation in the seston C:N ratio of the Arctic Ocean and pan-Arctic shelves. *J Mar Sys* **129**: 214–223. DOI: https://doi.org/10.1016/j.jmarsys.2013.06.004

**Geider, R** and **La Roche, J** 2002 Redfield revisited: variability of C:N:P in marine microalgae and its biochemical basis. *Eur J Phycol* **37**(1): 1–17. DOI: https://doi.org/10.1017/S0967026201003456

**Hales, B, Moum, JN, Covert, P** and **Perlin, A** 2005 Irreversible nitrate fluxes due to turbulent mixing in a coastal upwelling system. *JGR: Oceans* **110**(C10): S11. DOI: https://doi.org/10.1029/2004JC002685

**Hodal, H** and **Kristiansen, S** 2008 The importance of small-celled phytoplankton in spring blooms at the marginal ice zone in the northern Barents Sea. *Deep-Sea Res II* **55**(20–21): 2176–2185. DOI: https://doi.org/10.1016/j.dsr2.2008.05.012

**Holm-Hansen, O** and **Riemann, B** 1978 Chlorophyll *a* Determination: Improvements in Methodology. *Oikos* **30**(3): 438–447. DOI: https://doi.org/10.2307/3543338

**IPCC** (ed.) 2013 *Climate Change 2013: The Physical Science Basis. Contribution of Working Group I to the Fifth Assessment Report of the Intergovernmental Panel on Climate Change.* Cambridge, United Kingdom and New York, NY, USA: Cambridge University Press.

**Iversen, MH** and **Ploug, H** 2013 Temperature effects on carbon-specific respiration rate and sinking velocity of diatom aggregates – potential implications for deep ocean export processes. *Biogeosciences* **10**(6): 4073–4085. DOI: https://doi.org/10.5194/bg-10-4073-2013

**Johnson, KS** and **Coletti, LJ** 2002 In situ ultraviolet spectrophotometry for high resolution and long-term monitoring of nitrate, bromide and bisulfide in the ocean. *Deep-Sea Res I* **49**(7): 1291–1305. DOI: https://doi.org/10.1016/S0967-0637(02)00020-1

**Kaplunenko, DD, Lobanov, VB, Tishchenko, PY** and **Shvetsova, MG** 2013 Nitrate in situ measurements in the northern Japan Sea. *Deep-Sea Res Pt II* **86–87**: 10–18. DOI: https://doi.org/10.1016/j.dsr2.2012.08.005

**Kvingedal, B** 2005 Sea-Ice Extent and Variability in the Nordic Seas, 1967–2002. In: Drange, H, Dokken, T, Furevik, T, Gerdes, R and Berger, W (eds.), *The Nordic Seas: An Integrated Perspective*, 39–49. Washington, D. C.: American Geophysical Union.

**Le Fouest, V, Postlethwaite, C, Morales Maqueda, MA, Bélanger, S** and **Babin, M** 2011 On the role of tides and strong wind events in promoting summer primary production in the Barents Sea. *Cont Shelf Res* **31**(17): 1869–1879. DOI: https://doi.org/10.1016/j.csr.2011.08.013

**Leu, E, Søreide, JE, Hessen, DO, Falk-Petersen, S** and **Berge, J** 2011 Consequences of changing sea-ice cover for primary and secondary producers in the European Arctic shelf seas: Timing, quantity, and quality. *Progr Oceanogr* **90**(1–4): 18–32. DOI: https://doi.org/10.1016/j.pocean.2011.02.004

**Loeng, H** 1991 Features of the physical oceanographic conditions of the Barents Sea. *Polar Res* **10**(1): 5–18. DOI: https://doi.org/10.1111/j.1751-8369.1991.tb00630.x

**Louanchi, F** and **Najjar, RG** 2001 Annual cycles of nutrients and oxygen in the upper layers of the North Atlantic Ocean. *Deep-Sea Res II* **48**(10): 2155–2171. DOI: https://doi.org/10.1016/S0967-0645(00)00185-5

**Mann, K** and **Lazier, J** 2006 *Dynamics of Marine Ecosystems: Biological-Physical Interactions in the Oceans*, Third Edition. Blackwell Publishing.

**Martin, AP, Lucas, MI, Painter, SC, Pidcock, R, Prandke, H,** et al. 2010a The supply of nutrients due to vertical turbulent mixing: A study at the Porcupine Abyssal Plain study site in the northeast Atlantic. *Deep-Sea Res II* **57**(15): 1293–1302. DOI: https://doi.org/10.1016/j.dsr2.2010.01.006

**Martin, J, Tremblay, J-É, Gagnon, J, Tremblay, G, Lapoussiére, A,** et al. 2010b Prevalence, structure and properties of subsurface chlorophyll maxima in Canadian Arctic waters. *Mar Ecol Prog Ser* **412**: 69–84. DOI: https://doi.org/10.3354/meps08666

**Martin, J, Tremblay, J-È** and **Price, NM** 2012 Nutritive and photosynthetic ecology of subsurface chlorophyll maxima in Canadian Arctic waters. *Biogeosciences* **9**: 5353–5371. DOI: https://doi.org/10.5194/bg-9-5353-2012

**Mei, ZP, Legendre, L, Tremblay, JÉ, Miller, LA, Gratton, Y,** et al. 2005 Carbon to nitrogen (C:N) stoichiometry of the spring–summer phytoplankton bloom in the North Water Polynya (NOW). *Deep-Sea Res I* **52**(12): 2301–2314. DOI: https://doi.org/10.1016/j.dsr.2005.07.001

**Moum, JN** 1996 Efficiency of mixing in the main thermocline. *J Geophys Res* **101**(C5): 12057–12069. DOI: https://doi.org/10.1029/96JC00508

**Olli, K, Rieser, CW, Wassmann, P, Ratkova, T, Arashkevich, E,** et al. 2002 Seasonal variation in vertical flux of biogenic matter in the marginal ice zone and the central Barents Sea. *J Mar Syst* **38**: 189–204. DOI: https://doi.org/10.1016/S0924-7963(02)00177-X

**Omand, MM** and **Mahadevan, A** 2015 The shape of the oceanic nitracline. *Biogeosciences* **12**(11): 3273–3287. DOI: https://doi.org/10.5194/bg-12-3273-2015

**Osborn, TR** 1980 Estimates of the Local Rate of Vertical Diffusion from Dissipation Measurements. *J Phys Oceanogr* **10**(1): 83–89. DOI: https://doi.org/10.1175/1520-0485(1980)010<0083:EOTLRO>2.0.CO;2

Art. 43, page 14 of 15

Wiedmann et al: Upward nitrate flux and downward particulate organic carbon flux under contrasting situations of stratification and turbulent mixing in an Arctic shelf sea

**Painter, SC, Henson, SA, Forryan, A, Steigenberger, S, Klar, J,** et al. 2014 An assessment of the vertical diffusive flux of iron and other nutrients to the surface waters of the subpolar North Atlantic Ocean. *Biogeosciences* **11**(8): 2113–2130. DOI: https://doi.org/10.5194/bg-11-2113-2014

**Platt, T, Gallegos, CL** and **Harrison, WG** 1980 Photoinhibition of photosynthesis in natural assemblages of marine phytoplankton. *J Mar Res* **38**: 687–701.

**Prandke, H** and **Stips, A** 1998 Test measurements with an operational microstructure-turbulence profiler: Detection limit of dissipation rates. *Aquat Sci* **60**(3): 191–209. DOI: https://doi.org/10.1007/s000270050036

**Rainville, L, Lee, CM** and **Woodgate, RA** 2011 Impact of wind-driven mixing in the Arctic Ocean. *Oceanography* **24**(3): 136. DOI: https://doi.org/10.5670/oceanog.2011.65

**Randelhoff, A, Fer, I, Sundfjord, A, Tremblay, J-É** and **Reigstad, M** 2016 Vertical fluxes of nitrate in the seasonal nitracline of the Atlantic sector of the Arctic Ocean. *JGR: Oceans* **121**(7): 5282–5295. DOI: https://doi.org/10.1002/2016JC011779

**Redfield, AC** 1934 On the proportion of organic derivates in sea water and their relation to the composition of plankton. *James Johnstone Memorial Volume,* 177–192. Liverpool: Liverpool University Press.

**Redfield, AC** 1958 The biological control of chemical factors in the environment. *Am Sci* **46**(3): 205–221.

**Reigstad, M, Riser, CW, Wassmann, P** and **Ratkova, T** 2008 Vertical export of particulate organic carbon: Attenuation, composition and loss rates in the northern Barents Sea. *Deep-Sea Res II* **55**: 2308–2319. DOI: https://doi.org/10.1016/j.dsr2.2008.05.007

**Reigstad, M** and **Wassmann, P** 2007 Does *Phaeocystis* spp. contribute significantly to vertical export of organic carbon? *Biogeochemistry* **83**(1–3): 217–234. DOI: https://doi.org/10.1007/s10533-007-9093-3

**Reigstad, M, Wassmann, P, Wexels Riser, C, Øygarden, S** and **Rey, F** 2002 Variations in hydrography, nutrients and chlorophyll a in the marginal ice-zone and the central Barents Sea. *J Mar Syst* **38**(1–2): 9–29. DOI: https://doi.org/10.1016/S0924-7963(02)00167-7

**Sakshaug, E, Johnsen, G, Kristiansen, S, von Quillfeldt, C, Rey, F,** et al. 2009 Phytoplankton and primary production. In: Sakshaug, E, Johnsen, G and Kovacs, K (eds.), *Ecosystem Barents Sea,* 167–208. Trondheim, Norway: Tapir Academic Press.

**Sakshaug, E, Kristiansen, S** and **Syvertsen, E** 1991 Planktonalger. In: Sakshaug, E, Bjørge, A, Gulliksen, F, Loeng, H and Melhum, F (eds.), *Økosystem Barentshav.* Oslo: Universitetsforlaget.

**Sakshaug, E** and **Slagstad, D** 1992 Sea ice and wind: Effects on primary productivity in the Barents Sea. *Atmos Ocean* **30**(4): 579–591. DOI: https://doi.org/10.1080/07055900.1992.9649456

**Sambrotto, RN, Niebauer, HJ, Goering, JJ** and **Iverson, RL** 1986 Relationships among vertical mixing, nitrate uptake, and phytoplankton growth during the spring bloom in the southeast Bering Sea middle shelf. *Cont Shelf Res* **5**(1–2): 161–198. DOI: https://doi.org/10.1016/0278-4343(86)90014-2

**Sharples, J, Tweddle, JF, Mattias Green, J, Palmer, MR, Kim, Y-N,** et al. 2007 Spring-neap modulation of internal tide mixing and vertical nitrate fluxes at a shelf edge in summer. *Limnol Oceanogr* **52**(5): 1735–1747. DOI: https://doi.org/10.4319/lo.2007.52.5.1735

**Shiozaki, T, Ijichi, M, Isobe, K, Hashihama, F, Nakamura, K-i,** et al. 2016 Nitrification and its influence on biogeochemical cycles from the equatorial Pacific to the Arctic Ocean. *ISME J* **10**(9): 2184–2197. DOI: https://doi.org/10.1038/ismej.2016.18

**Slagstad, D** and **McClimans, TA** 2005 Modeling the ecosystem dynamics of the Barents sea including the marginal ice zone: I. Physical and chemical oceanography. *J Mar Sys* **58**(1–2): 1–18. DOI: https://doi.org/10.1016/j.jmarsys.2005.05.005

**South, GR** and **Whittick, A** 1987 *An Introduction to Phycology.* Wiley-Blackwell.

**Sundfjord, A, Fer, I, Kasajima, Y** and **Svendsen, H** 2007 Observations of turbulent mixing and hydrography in the marginal ice zone of the Barents Sea. *J Geophys Res-Oceans* **112**(C5): 008. DOI: https://doi.org/10.1029/2006JC003524

**Torres-Valdés, S, Tsubouchi, T, Bacon, S, Naveira-Garabato, AC, Sanders, R,** et al. 2013 Export of nutrients from the Arctic Ocean. *J Geophys Res-Oceans* **118**(4): 1625–1644. DOI: https://doi.org/10.1002/jgrc.20063

**Tremblay, J-É, Anderson, LG, Matrai, P, Coupel, P, Bélanger, S,** et al. 2015 Global and regional drivers of nutrient supply, primary production and $CO_2$ drawdown in the changing Arctic Ocean. *Prog Oceanogr* **139**: 171–196. DOI: https://doi.org/10.1016/j.pocean.2015.08.009

**Tremblay, J-É, Michel, C, Hobson, KA, Gosselin, M** and **Price, NM** 2006 Bloom dynamics in early opening waters of the Arctic Ocean, *Limnol Oceanogr* **51**(2): 900–912. DOI: https://doi.org/10.4319/lo.2006.51.2.0900

**Turner, JT** 2002 Zooplankton fecal pellets, marine snow and sinking phytoplankton blooms. *Aquat Microb Ecol* **27**: 57–102. DOI: https://doi.org/10.3354/ame027057

**Turner, JT** and **Ferrante, JG** 1979 Zooplankton fecal pellets in aquatic ecosystems. *Bioscience* **29**(11): 670–677. DOI: https://doi.org/10.2307/1307591

**Wassmann, P** and **Reigstad, M** 2011 Future Arctic Ocean seasonal ice zones and implications for pelagic-benthic coupling. *Oceanography* **24**(3): 220–231. DOI: https://doi.org/10.6570/oceanog.2011.74

**Wexels Riser, C, Reigstad, M, Wassmann, P, Arashkevich, E** and **Falk-Petersen, S** 2007 Export or retention? Copepod abundance, faecal pellet production and vertical flux in the marginal ice zone through snap shots from the northern Barents Sea. *Polar Biol* **30**(6): 719–730. DOI: https://doi.org/10.1007/s00300-006-0229-z

Wiedmann et al: Upward nitrate flux and downward particulate organic carbon flux under contrasting situations of stratification and turbulent mixing in an Arctic shelf sea

Art. 43, page 15 of 15

**Wexels Riser, C, Wassmann, P, Reigstad, M** and **Seuthe, L** 2008 Vertical flux regulation by zooplankton in the northern Barents Sea during Arctic spring. *Deep-Sea Res II* **55**(20–21): 2320–2329. DOI: https://doi.org/10.1016/j.dsr2.2008.05.006

**Wiedmann, I, Reigstad, M, Sundfjord, A** and **Basedow, S** 2014 Potential drivers of sinking particle's size spectra and vertical flux of particulate organic carbon (POC): Turbulence, phytoplankton, and zooplankton. *J Geophys Res-Oceans* **119**(10): 6900–6917. DOI: https://doi.org/10.1002/2013JC009754

**Yamazaki, H** and **Osborn, T** 1990 Dissipation estimates for stratified turbulence. *J Geophys Res* **95**(C6): 9739–9744. DOI: https://doi.org/10.1029/JC095iC06p09739